A multiphysics model for ultra-high frequency optomechanical resonators optically actuated and detected in the oscillating mode

S Sbarra, P E Allain, S Suffit, A Lemaître, I Favero

A multiphysics model for ultra-high frequency optomechanical resonators optically actuated and detected in the oscillating mode

S. Sbarra,[1] P. E. Allain,[1] S. Suffit,[1] A. Lemaître,[2] and I. Favero[1, a)]

[1)]*Matériaux et Phénomènes Quantiques, Université de Paris, CNRS, UMR 7162, 10 rue Alice Domon et Léonie Duquet, Paris 75013, France*

[2)]*Centre de Nanosciences et de Nanotechnologies, CNRS, UMR 9001, Université Paris-Saclay, Palaiseau 91120, France*

Optomechanical systems combine extreme sensitivity and bandwidth in the control of mechanical motion, of interest for various applications. Integrated on a chip, actuated and detected all-optically by a single laser, they could disrupt sensing technologies. We introduce here a multiphysics model that describes their operation in the oscillating mode, under sinusoidal modulation of the laser, when both photothermal forces and radiation pressure/electrostriction are present, and when (non)linear absorption occurs in the device. The model is validated by systematic experiments on ultra-high frequency optomechanical disk resonators and leads to a quantitative assessment of the amplitude and phase of the demodulated output signal, which carries the sensing information.

The small dimensions of mechanical micro- and nano-resonators induces a large responsivity to external perturbations, making these systems ideal for sensing purposes[1,2]. Actuation of the mechanical system is necessary to increase the vibration amplitude and improve its sensing performances[3,4]. Among multiple actuation mechanisms, optical driving of mechanical resonators enables broadband actuation up to the GHz mechanical frequency range. At the same time, optical techniques permit ultrasensitive, eventually quantum-limited, detection of motion. For these reasons, several optomechanical devices[5,6] have been pushed forward for magnetic field[7], mass[8,9,10,11] or atomic force sensing[12,13]. Driving and detecting the mechanical sensor in an all-optical way, with a single laser source, offers an obvious advantage of simplicity, well suited for integration. The oscillating sensing mode, where the mechanical system is sinusoidally forced, is then obtained under coherent modulation of the laser, while the output light is demodulated.

Early experiments in optomechanics, while not aiming at sensing, did implement such modulation/demodulation approach in order to characterize the dynamical response of the system under study[14,15]. In [15], the effect of photothermal forces, where photons are absorbed and thermally distort the mechanical system, was considered within a delayed force model. The latter efficiently depicted the behaviour of employed cantilevers of mechanical frequency $\omega_m = 2\pi \times 10$kHz, but was inadequate for high frequency devices operating in the good cavity limit $\omega_m \gtrsim \kappa$ with κ the optical cavity decay rate[16]. In contrast, the canonical optomechanical radiation-pressure model[6] correctly works at arbitrary high mechanical frequency, and modulation/demodulation experiments in this regime have been popularized as being the optomechanical analogue of electromagnetically induced transparency[17,18]. Unfortunately, the latter model neglects photothermal interactions, which are often sizable at room temperature and of concrete importance for operational optomechanical sensors[19,20,21]. In a recent paper[22], a model was introduced that solved for that discrepancy by writing three coupled equations for the cavity mode, the mechanical and thermal degrees of freedom of a resonator, allowing quantitative modelling of dynamical backaction effects at ultra-high frequency with significant photothermal interactions. Despite its prime importance for sensing, the oscillating mode with a sinusoidally-forced resonator was however not treated in this latter work. This is done here, where the model of[22] is extended and solved in the case of a modulated input laser and demodulated output optical signal. We derive compact analytical expressions for both quadratures of the demodulated signal, including in a regime where nonlinear absorption is present, giving rise to a nonlinear component of the optical force. We confront these expressions to systematic experiments on optomechanical disk resonators with mechanical modes in the ultra-high frequency range, varying the modulation frequency, the optical operating conditions such as detuning and power, and the investigated mechanical modes. The validation of the tested model prepares the ground for the calibrated use of integrated oscillating optomechanical sensors optically operated at room temperature, a required step for concrete applications.

A electron micrograph of the optomechanical system under investigation is shown in Fig. 1 (a). It consists of a Gallium Arsenide (GaAs) disk patterned on an GaAs(200 nm)/$Al_{0.8}Ga_{0.2}As$(1800 nm)/GaAs(substrate) epitaxial wafer using e-beam lithography and inductively coupled plasma etching. Hydrofluoric acid under-etching is employed to selectively remove the AlGaAs and shape the disk pedestal. This structure supports optical whispering gallery modes (WGMs) that can be excited via an integrated suspended waveguide at a rate κ_{ex} (Fig. 1 (b)). Radiative contributions to the WGM cavity losses (bending and scattering losses) are grouped under the rate κ_{rad}. Intracavity photons are absorbed at a rate κ_{abs}. As depicted in Fig. 1 (c), a single telecom (sub-bandgap) photon can be absorbed in a transition involving a mid-gap state[23,24] (κ_{lin}), while a pair can be directly absorbed by two-photon absorption (κ_{TPA}), such that $\kappa_{abs} = \kappa_{lin} + \kappa_{TPA}$. Both effects, linear and nonlinear in the circulating power, are responsible for heating up the resonator. For a ΔT temperature increase of the disk, the local

[a)]ivan.favero@u-paris.fr;

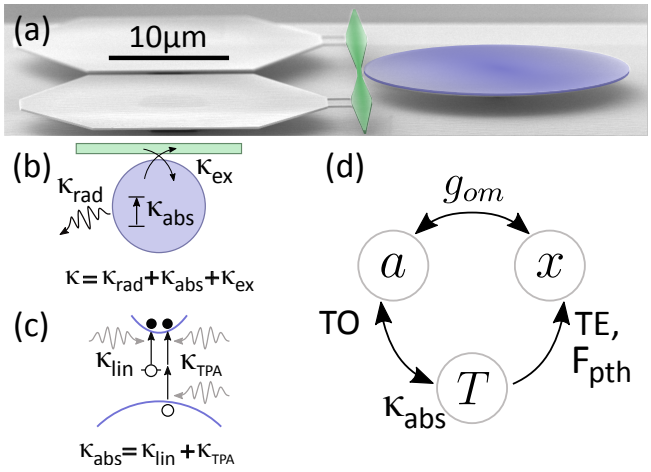

FIG. 1. (a) Electron micrograph: GaAs optomechanical disk (blue) in the vicinity of its coupling waveguide (green), whose extremities are tapered for efficient light injection and collection. The guide is supported by two hexagonal holding pads (left), which play no optical nor mechanical role. (b) Three contributions to the optical cavity loss rate (κ): the radiative losses ($\kappa_{\rm rad}$), coupling rate to the waveguide ($\kappa_{\rm ex}$) and absorption losses ($\kappa_{\rm abs}$). (c) Linear absorption ($\kappa_{\rm lin}$) involves single telecom photon processes, while two-photon absorption TPA ($\kappa_{\rm TPA}$) involves pairs of photons. (d) Optical, mechanical and thermal degrees of freedom in interaction (see text).

stress induced by thermal expansion is given by[25]:

$$\sigma_{ij}^{th} = C_{ijkl}\beta_{\rm th}\delta_{kl}\Delta T \tag{1}$$

with C_{ijkl} the stiffness tensor and $\beta_{\rm th}$ the thermal expansion coefficient of the material. Each mechanical mode of the resonator is impacted its own way by this thermal stress. In a lumped element model associated to a given mechanical mode, the effective mass on a spring is subjected to a photothermal force $F_{\rm pth}$, whose amplitude is given by[25]:

$$F_{\rm pth} = \int_V dV\,\sigma_{ij}^{th} S_{ij} = \alpha \times \Delta T \tag{2}$$

where S_{ij} is the strain field of the considered mechanical mode. Another consequence of the temperature increase in the disk is the red-shift of optical and mechanical resonances. The first is a consequence of the thermo-optic effect (TO) while the second is related to the thermo-elastic (TE) softening of the material at high temperature. When combined with the canonical optomechanical coupling between the motion x and the optical cavity field a, these various thermal effects give rise to a close set of interactions between optical, mechanical and thermal degrees of freedom (Fig. 1 (d)), governed by three coupled equations:

$$\begin{aligned}
\dot{a} &= -\frac{\kappa}{2}a + i\left(\Delta + g_{\rm om}x + \frac{\omega_{\rm cav}}{n_g}\frac{dn_{eff}}{dT}\Delta T\right)a + \sqrt{\kappa_{\rm ex}}a_{\rm in}, \\
m_{\rm eff}\ddot{x} + m_{\rm eff}\Gamma_{\rm m}\dot{x} + m_{\rm eff}\omega_m^2 x &= F_{\rm pth} + F_{\rm opt}, \\
\Delta\dot{T} &= -\frac{1}{\tau_{\rm th}}\left(\Delta T - R_{\rm th}\kappa_{\rm abs}\hbar\omega_{\rm L}|a|^2\right),
\end{aligned} \tag{3}$$

with $\Delta = \omega_{\rm L} - \omega_{\rm cav}$ the laser-cavity detuning, $g_{\rm om} = -\partial\omega_{\rm cav}/\partial x$ the optomechanical frequency-pull parameter, n_g and dn_{eff}/dT being respectively the effective group refractive index and thermo-optic coefficient. Optical fields are written in the rotating frame. $|a|^2$ is normalized to the number of photons in the cavity and $a_{\rm in}$ such that $\hbar\omega_L|a_{\rm in}|^2$ is the input power in the waveguide. We chose a phase reference such that $\bar{a}$ ($\bar{a}_{in}$) is real (complex) valued. $m_{\rm eff}$, $\Gamma_{\rm m}$ and $\omega_{\rm m}$ are the mechanical resonator's effective mass, damping rate and (temperature-dependent through TE) resonant frequency. Forces acting on the mass include a photothermal ($F_{\rm pth}$) and a radiation pressure and electrostrictive ($F_{\rm opt}$) contribution. The latter is given by as $F_{\rm opt} = \hbar g_{\rm om}|a|^2$, where $g_{\rm om}$ is calculated numerically considering both the geometrical and photoelastic coupling[26]. $R_{\rm th}$ and $\tau_{\rm th}$ are the thermal resistance and relaxation time of the resonator. This model serves as a starting point to describe modulation/demodulation experiments of interest for sensing in the oscillating mode.

Fig. 2 shows the experimental set-up employed to perform optical actuation and detection of the mechanical device previously described. The light of a tunable telecom laser is amplitude-modulated by a Mach-Zehnder electro-optic modulator (EOM), generating two side-bands in the input field[27]: $a_{\rm in}(t) = \bar{a}_{\rm in}\left(1 + \beta/2e^{+i\Omega t} + \beta/2e^{-i\Omega t}\right)$, where Ω and β are the modulation angular frequency and depth. Two microlensed fibers provide injection into and collection from the waveguide coupled to the disk, where a TE or TM WGM is excited depending on the polarization controller (PC) selection. The intracavity field response to the modulation is[17]: $a(t) = \bar{a} + \delta a(t)$ with $\delta a(t) = A^- e^{-i\Omega t} + A^+ e^{+i\Omega t}$, while we write the displacement and temperature increase: $x(t) = \bar{x} + \delta x(t), \Delta T(t) = \overline{\Delta T} + \delta T(t)$ with $\delta x(t) = Xe^{-i\Omega t} + X^* e^{+i\Omega t}$ and $\delta T(t) = \Delta T_c e^{-i\Omega t} + \Delta T_c^* e^{+i\Omega t}$. The steady-state value of the fields are given by: $\bar{a} = \sqrt{\kappa_{\rm ex}}\bar{a}_{\rm in}/(\kappa/2 - i\bar{\Delta})$, $\bar{x} = (\bar{F}_{\rm opt} + \bar{F}_{\rm pth})/(m_{\rm eff}\omega_{\rm m}^2)$, $\overline{\Delta T} = R_{\rm th}(\kappa_{\rm lin} + \bar{\kappa}_{\rm TPA})\hbar\omega_{\rm L}|\bar{a}|^2$, with $\bar{\Delta} = \Delta + g_{\rm om}\bar{x} + \omega_{\rm cav}/n_g \times dn_{eff}/dT \times \overline{\Delta T}$ the detuning modified by the optomechanical coupling and the thermo-optic effect. The output optical signal is first amplified by an Erbium-doped fiber amplifier (EDFA) and converted into an electrical signal by a photo-detector (PD), which is then fed into an Ultra-High-Frequency (UHF) Lock-in Amplifier (LIA). This latter signal is proportional to the modulus squared of the output light field:

$$\begin{aligned}
|a_{\rm out}(t)|^2 = \Big|\bar{a}_{\rm in} - \sqrt{k_{\rm ex}}\bar{a} + \left(\frac{\beta}{2}\bar{a}_{\rm in} - \sqrt{k_{\rm ex}}A^-\right)e^{-i\Omega t} \\
+ \left(\frac{\beta}{2}\bar{a}_{\rm in} - \sqrt{k_{\rm ex}}A^+\right)e^{+i\Omega t}\Big|^2
\end{aligned} \tag{4}$$

which comprises a DC term and two additional components oscillating at Ω and 2Ω. The LIA demodulates this signal at Ω and decomposes it into an in-phase (I) and quadrature (Q) component:

$$\begin{aligned}
I &= Re\{(\bar{a}_{\rm in}^* - \sqrt{\kappa_{\rm ex}}\bar{a})(\bar{a}_{\rm in}\beta - \sqrt{\kappa_{\rm ex}}(A^- + A^+))\} \\
Q &= Im\{(\bar{a}_{\rm in}^* - \sqrt{\kappa_{\rm ex}}\bar{a})(\sqrt{\kappa_{\rm ex}}(A^- - A^+))\}
\end{aligned} \tag{5}$$

or into an amplitude ($R = \sqrt{I^2 + Q^2}$) and phase ($\theta = \arctan(Q/I)$). Injecting the field ansatz into the governing

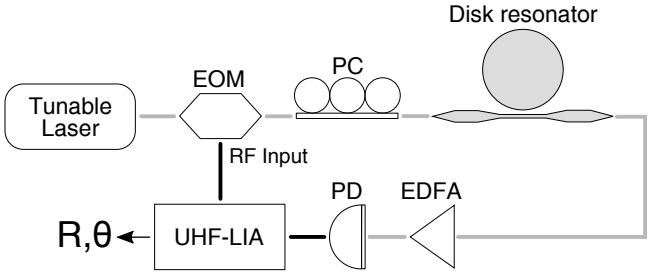

FIG. 2. Experimental setup of the all-optical actuation/detection of mechanical motion. The amplitude of the laser power is modulated by an electro-optic modulator (EOM). The polarization is selected with a polarization controller (PC). Light is injected into the integrated waveguide evanescently coupled to the disk resonator, and then collected and amplified by an Erbium-doped Fiber Amplifier (EDFA). The signal is converted into current by a high-bandwidth photo-detector (PD) and finally sent to a Ultra-High Frequency Lock-in Amplifier (UHF-LIA), where it is mixed with the reference signal.

equations, we find:

$$A^{+}(\Omega) = \frac{i}{2}\frac{2\phi(\Omega+\bar{\Delta}-i\kappa/2)+(\phi+\phi^{*})(\zeta_{\rm opt}^{*}+\zeta_{\rm th}^{*})}{\bar{\Delta}^{2}+\bar{\Delta}(\zeta_{\rm opt}^{*}+\zeta_{\rm th}^{*})-(\Omega-i\kappa/2)^{2}} \quad (6)$$

$$A^{-}(\Omega) = \frac{i}{2}\frac{2\phi(-\Omega+\bar{\Delta}-i\kappa/2)+(\phi+\phi^{*})(\zeta_{\rm opt}+\zeta_{\rm th})}{\bar{\Delta}^{2}+\bar{\Delta}(\zeta_{\rm opt}+\zeta_{\rm th})-(\Omega+i\kappa/2)^{2}} \quad (7)$$

with $\phi = \sqrt{\kappa_{\rm ex}}\bar{a}_{\rm in}\beta/2$, $\zeta_{opt} = 2\bar{a}^{2}\hbar g_{\rm om}^{2}\chi(\Omega)$, $\zeta_{th} = 2\bar{a}^{2}(\omega_{\rm cav}/n_{g} \times dn_{eff}/dT + \alpha g_{\rm om}\chi(\Omega))R_{\rm th}\hbar\omega_{\rm L}(\kappa_{\rm lin} + 2\bar{\kappa}_{\rm TPA})(1-i\Omega\tau_{\rm th})^{-1}$, ϕ^{*}, $\zeta_{\rm opt}^{*}$ and $\zeta_{\rm pth}^{*}$ their complex conjugates, and $\chi(\Omega) = \left[m_{\rm eff}(\omega_{\rm m}^{2}-\Omega^{2}-i\Omega\Gamma_{\rm m})\right]^{-1}$ the mechanical susceptibility. When thermal effects are switched off, and under the approximation of a single sideband in the input field, Eqs. 6 and 7 lead back to the results established in the context of optomechanically induced transparency[17]. Expressions for ΔT_c and X are given in the supplementary material.

With the model now in hands, we start by presenting results of modulation/demodulation both at low frequency (10 kHz-100 MHz) and at high frequency, close to the first order Radial Breathing Mode (RBM1), whose resonant frequency is located at 132 MHz for the present disk (11 μm radius, 200 nm thickness). An optical power of 200 μW is injected in the integrated waveguide and the laser wavelength is tuned to the blue flank of the optical WGM resonance ($\Delta > 0$). (Note that systematic measurements on the red-detuned flank could not be completed because of limiting thermo-optic instabilities). When sweeping the modulation frequency from 10 kHz to 100 MHz, a dip in the phase and a decrease in the amplitude appear in the demodulated signal (Fig. 3 (a)), as consequence of a thermal phase lag. Indeed, as apparent in the first line of Eq. 3, the thermo-optic effect, just as the canonical optomechanical coupling, modifies the amplitude and the phase of the cavity optical field. Being a consequence of photon absorption, the former is filtered by the thermal response of the device (in the microsecond range), and hence distinguishable from the latter. Much larger amplitude and phase

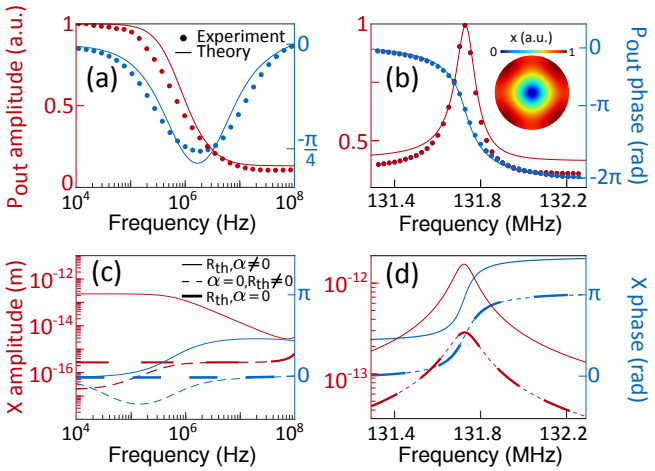

FIG. 3. Amplitude and (unwrapped) phase response function of the demodulated optical signal when the modulation frequency is swept between 10 kHz and 100 MHz (a) and around the mechanical resonance frequency of RBM1 (b). The mode profile of RBM1 is in inset. The amplitude is normalized by its maximum value over the frequency span. (c),(d): X deduced from the model. The solid line represents the results obtained with the full model when photothemal forces and heating are present ($\alpha \neq 0$, $R_{\rm th} \neq 0$), while the thin and thick dashed lines represents respectively the case where photothermal forces ($\alpha = 0$) and heating of the resonator ($R_{\rm th}, \alpha = 0$) are switched off.

shifts in the demodulated signal are however found closer to the resonant frequency of the RBM1 (Fig. 3 (b)), whose mode profile is shown in the inset. The photothermal force DC amplitude is three orders of magnitude larger than radiation pressure ($\alpha R_{\rm th}\omega_{\rm cav}\bar{\kappa}_{\rm abs}/g_{\rm om} = 3\times10^{3}$), which contributes to an efficient driving of motion even at the frequency of RBM1. The experimental results of Fig. 3 (a) and (b) are well reproduced by the model introduced above (Eqs. 6,7) (solid line), when using the parameters listed in Table I. The vast majority of these parameters have been independently measured or calculated with finite element method (FEM), while $\tau_{\rm th}$ has been obtained from the fit of the low frequency region ($\leq$100 MHz) (Fig. 3 (a)) and found to be consistent with the FEM value. The amplitude of the absorptive effects, parametrized by $\kappa_{\rm lin}$, $\kappa_{\rm TPA}$ and $R_{\rm th}$, was obtained by fitting the thermo-optic shift and distortion of the WGM resonance[23] (see supplementary material). The nonlinear absorption rate is proportional to the TPA coefficient $\beta_{\rm TPA}$[28]:

$$\kappa_{\rm TPA} = \frac{\Gamma_{\rm TPA}\beta_{\rm TPA}c^{2}}{V_{\rm TPA}n_{g}^{2}}\hbar\omega_{\rm L}|a|^{2} \quad (8)$$

with $\Gamma_{\rm TPA}$ and $V_{\rm TPA}$ the TPA confinement factor and volume, c the speed of light and $n_{\rm g}$ the group index. With all parameters of Table I fixed this way, the fit of the response in the high frequency region is obtained with no additional adjustable parameter (Fig. 3 (b)).

To better appreciate the relative contributions of the photothermal force and radiation pressure/electrostriction in our experiments, in Fig. 3 (c,d) we extract from our model the mechanical displacement modulation component X as func-

TABLE I. Model Parameters

Parameter	Value	Units	Source
$\omega_{cav}/(2\pi)$	1.93×10^{14}	Hz	measured
$\kappa_{rad}/(2\pi)$	1.62	GHz	measured
$\kappa_{ext}/(2\pi)$	1.27	GHz	measured
$\kappa_{lin}/(2\pi)$	0.13	GHz	measured
β_{TPA}	30	cm GW^{-1}	fit and [29,30,31]
Γ_{TPA}	0.9994	-	FEM (based on [28])
V_{TPA}	2.42×10^{-17}	m^3	FEM (based on [28])
n_g	3.47	-	Effective Index Method ref.[32], and FEM
P_{in}	210	μW	measured
2β	6.87%		measured
dn$_{eff}$/dT	2.35×10^{-4}	K^{-1}	Effective Index Method, refs.[33,32], and FEM
$g_{om}/(2\pi)$	2.34×10^{19}	Hz m^{-1}	FEM (based on [34,26])
m_{eff}	255	pg	FEM (based on [34,26])
ω_m	$2\pi\times131.7$	MHz	measured
Γ_m	$2\pi\times135$	kHz	measured
α	7.83	μN K^{-1}	FEM (based on[25])
τ_{th}	3.99	μs	fit and FEM (based on[22])
R_{th}	5.64×10^4	K W^{-1}	fit and FEM (based on[22])
β_{th}	5.7×10^{-6}	K $^{-1}$	ref.[35]
$\bar{\Delta}/(2\pi)$	0.5	GHz	measured

tion of the modulation frequency (solid line) and compare it to situations where the photothermal forces only are switched-off (thin dashed line, $\alpha=0$) and where all thermal effects are switched off (thick dashed line, α, $R_{th}=0$). At frequencies below 10^6 Hz the amplitude of X is three order of magnitude larger when the photothermal force is present (Fig. 3 (c)). It reduces above the thermal frequency ($\sim10^6$ Hz), following a first-order filter function. At the same time, a $\pi/2$ phase lag is present at modulation frequencies higher than 10^6 Hz, which disappears when thermal effects are switched off. At even higher frequency, close to the mechanical resonance, the X amplitude also increases by a decade when the photothermal force is present ($\alpha\neq0$), despite the two order of magnitudes difference between thermal and mechanical frequencies (Fig. 3 (d)). A π phase shift is retrieved in X when scanning over the mechanical resonance, in accordance with an harmonic oscillator response. This overall behavior is consistent with that of a damped mechanical oscillator driven by two forces, radiation pressure/electrostriction and photothermal, of different intensity and response function.

In order to further test the validity of our model, which includes a photothermal force that has both linear and nonlinear components in the number of photons, we now systematically vary the incident optical power and the laser-cavity detuning. Figure 4 reports the amplitude and phase response of the demodulated optical signal at the RBM1 resonance frequency, as a function of the power (a,b) and detuning (c,d). When the number of intracavity photons increases, i.e. at larger power and/or smaller detuning, the red-shift of the mechanical resonance due to thermal softening of the material becomes visible. Here again, the full model (solid line) reproduces well the experimental data, all over the explored range. For the largest power and smaller detuning, TPA is twice as large as linear absorption. In this regime, it is responsible for increasing the cavity line width and gives rise to a dominating nonlinear photothermal force. For a given optical power and detuning, the oscillation amplitude can be enhanced by increasing the modulation depth (β). This generally results in improved performances for sensing applications. Measurements of the frequency stability of our optomechanical disk sensor down to 10^{-7} are shown in the supplementary material.

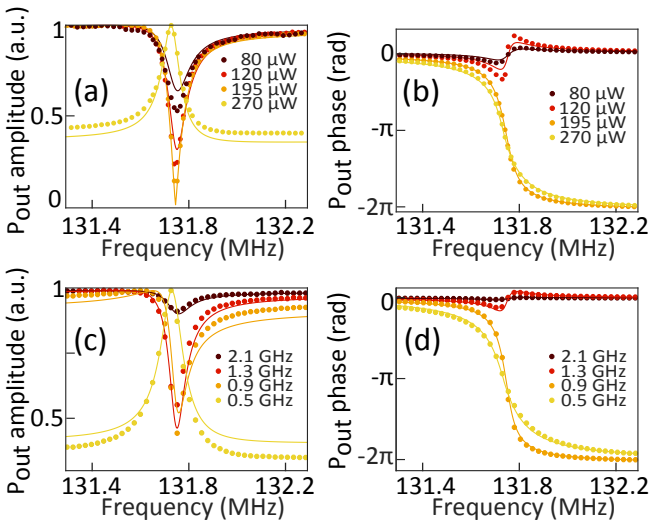

FIG. 4. Amplitude and (unwrapped) phase response function of the demodulated optical signal when the modulation frequency is swept around the mechanical resonance frequency of RBM1 for different input powers (a,b) and laser-cavity detuning (c,d). Amplitude is normalized with respect to its maximum value over the frequency span. Dots represent experimental data while the model is shown as a solid line.

The model presented here can be applied to any mechanical mode of a sensor, by using the proper mechanical susceptibility, proper optomechanical coupling, and proper photothermal force. In Fig. 5 we report experimental data acquired on the second order RBM (RBM2), together with the fit by the model. Both the peak amplitude and phase jump are smaller with respect to those of RBM1. This is the consequence of a lower mechanical quality factor ($Q_{RBM2}/Q_{RBM1}=0.4$) and of an increased spectral distance to the thermal cut-off frequency, which reduces the photothermal actuation efficiency. Similar data and analysis on a yet different category of mechanical modes, called the wine glass modes, are reported in the Supplementary Material.

In conclusion, we have developed and systematically tested a model that correctly depicts all-optical actuation and detection of optomechanical devices operating at ultra-high frequency in the oscillating mode. In contrast to prior models, it does account for photothermal forces, both linear and nonlinear, while also embedding radiation pressure and electrostrictive effects, without limitation on the mechanical frequency range. These features are essential for a precise description of chip-based semiconductor optomechanical sensors work-

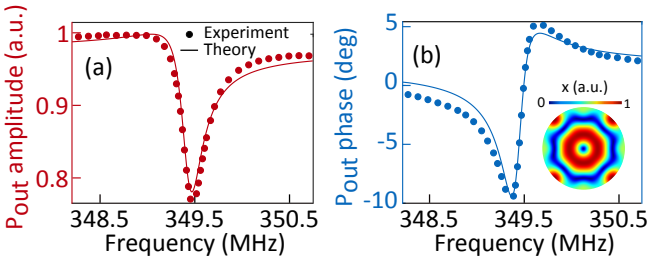

FIG. 5. Amplitude (a) and phase (b) response function of the demodulated optical signal at RBM2 resonance frequency. The amplitude is normalized with respect to its maximum value over the frequency span. Dots represent experimental data, while the model is shown as a solid line. The RBM2 displacement profile is reported in inset.

ing at room temperature, which are currently under development. Their modelling will enable the accurate interpretation of the demodulated sensor output when a physical signal (to be detected) triggers its response.

I. SUPPLEMENTARY MATERIAL

See Supplementary Material for the measurements of the device thermo-optic resonance shift, of the mechanical frequency stability, mechanical wine-glass modes, and for the derivation of X and ΔT_c.

ACKNOWLEDGMENTS

The authors acknowledge support from the European Commission through the VIRUSCAN (731868) FET-open and NOMLI (770933) ERC projects, and from the Agence Nationale de la Recherche through the Olympia and QuaSert projects.

II. DATA AVAILABILITY

The data that support the findings of this study are available from the corresponding authors upon reasonable request.

[1] M. S. Hanay, S. Kelber, A. K. Naik, D. Chi, S. Hentz, E. C. Bullard, E. Colinet, L. Duraffourg, and M. L. Roukes, "Single-protein nanomechanical mass spectrometry in real time," Nature Nanotechnology **7**, 602 (2012).

[2] E. Sage, M. Sansa, S. Fostner, M. Defoort, M. Gély, A. K. Naik, R. Morel, L. Duraffourg, M. L. Roukes, T. Alava, G. Jourdan, E. Colinet, C. Masselon, A. Brenac, and S. Hentz, "Single-particle mass spectrometry with arrays of frequency-addressed nanomechanical resonators," Nature Communications **9**, 3283 (2018).

[3] M. Sansa, E. Sage, E. C. Bullard, M. Gély, T. Alava, E. Colinet, A. K. Naik, L. G. Villanueva, L. Duraffourg, M. L. Roukes, G. Jourdan, and S. Hentz, "Frequency fluctuations in silicon nanoresonators," Nature Nanotechnology **11**, 552 (2016).

[4] K. L. Ekinci, Y. T. Yang, and M. L. Roukes, "Ultimate limits to inertial mass sensing based upon nanoelectromechanical systems," Journal of Applied Physics **95**, 2682–2689 (2004).

[5] I. Favero and K. Karrai, "Optomechanics of deformable optical cavities," Nature Photonics **3**, 201 (2009).

[6] T. J. &. M. Aspelmeyer, M., Kippenberg, "Cavity optomechanics," Reviews of Modern Physics **86** (2014).

[7] S. Forstner, S. Prams, J. Knittel, E. D. Van Ooijen, J. D. Swaim, G. I. Harris, A. Szorkovszky, W. P. Bowen, and H. Rubinsztein-Dunlop, "Cavity optomechanical magnetometer," Physical Review Letters **108**, 120801 (2012).

[8] F. Liu, S. Alaie, Z. C. Leseman, and M. Hossein-Zadeh, "Sub-pg mass sensing and measurement with an optomechanical oscillator," Optics Express **21**, 19555 (2013).

[9] W. Yu, W. C. Jiang, Q. Lin, and T. Lu, "Cavity optomechanical spring sensing of single molecules," Nature Communications **7**, 12311 (2016).

[10] M. Sansa, M. Defoort, A. Brenac, M. Hermouet, L. Banniard, A. Fafin, M. Gely, C. Masselon, I. Favero, G. Jourdan, and S. Hentz, "Optomechanical mass spectrometry," Nature Communications **11**, 3781 (2020).

[11] V. T. Sauer, Z. Diao, J. N. Westwood-Bachman, M. R. Freeman, and W. K. Hiebert, "Single laser modulated drive and detection of a nano-optomechanical cantilever," AIP Advances **7**, 015115 (2017).

[12] J. Chae, S. An, G. Ramer, V. Stavila, G. Holland, Y. Yoon, A. A. Talin, M. Allendorf, V. A. Aksyuk, and A. Centrone, "Nanophotonic Atomic Force Microscope Transducers Enable Chemical Composition and Thermal Conductivity Measurements at the Nanoscale," Nano Letters **17**, 5587 (2017).

[13] P. E. Allain, L. Schwab, C. Mismer, M. Gely, E. Mairiaux, M. Hermouet, B. Walter, G. Leo, S. Hentz, M. Faucher, G. Jourdan, B. Legrand, and I. Favero, "Optomechanical resonating probe for very high frequency sensing of atomic forces," Nanoscale **12**, 2939 (2020).

[14] A. Schliesser, P. Del'Haye, N. Nooshi, K. J. Vahala, and T. J. Kippenberg, "Radiation pressure cooling of a micromechanical oscillator using dynamical backaction," Physical Review Letters **97**, 243905 (2006).

[15] C. Metzger, I. Favero, A. Ortlieb, and K. Karrai, "Optical self cooling of a deformable Fabry-Perot cavity in the classical limit," Physical Review B **78**, 035309 (2008).

[16] J. Restrepo, J. Gabelli, C. Ciuti, and I. Favero, "Classical and quantum theory of photothermal cavity cooling of a mechanical oscillator," Comptes Rendus Physique **12**, 860 (2011).

[17] S. Weis, S. Deléglise, R. Rivière, E. Gavartin, O. Arcizet, A. Schliesser, and T. J. Kippenberg, "Optomechanically induced transparency," Science **330**, 1520 (2010).

[18] A. H. Safavi-Naeini, T. P. Alegre, J. Chan, M. Eichenfield, M. Winger, Q. Lin, J. T. Hill, D. E. Chang, and O. Painter, "Electromagnetically induced transparency and slow light with optomechanics," Nature **472**, 69 (2011).

[19] C. Belacel, Y. Todorov, S. Barbieri, D. Gacemi, I. Favero, and C. Sirtori, "Optomechanical terahertz detection with single meta-atom resonator," Nature Communications **8**, 1578 (2017).

[20] H. Zhu, F. Yi, and E. Cubukcu, "Plasmonic metamaterial absorber for broadband manipulation of mechanical resonances," Nature Photonics **10**, 709 (2016).

[21] B. Guha, P. E. Allain, A. Lemaître, G. Leo, and I. Favero, "Force Sensing with an Optomechanical Self-Oscillator," Physical Review Applied **14**, 024079 (2020).

[22] B. Guha, S. Mariani, G. Leo, I. Favero, and A. Lemaître, "High frequency optomechanical disk resonators in III-V ternary semiconductors," Optics Express **25**, 24639 (2017).

[23] D. Parrain, C. Baker, G. Wang, B. Guha, E. G. Santos, A. Lemaitre, P. Senellart, G. Leo, S. Ducci, and I. Favero, "Origin of optical losses in gallium arsenide disk whispering gallery resonators," Optics Express **23**, 19656 (2015).

[24] B. Guha, F. Marsault, F. Cadiz, L. Morgenroth, V. Ulin, V. Berkovitz, A. Lemaître, C. Gomez, A. Amo, S. Combrié, B. Gérard, G. Leo, and I. Favero, "Surface-enhanced gallium arsenide photonic resonator with quality factor of 6 × 1e6," Optica **4**, 218 (2017).

[25] I. Favero, "Optomechanical Interactions," in *Quantum Optomechanics and Nanomechanics, Lecture Notes of the Les Houches Summer School* (Oxford University Press, 2020).

[26] C. Baker, W. Hease, D.-T. Nguyen, A. Andronico, S. Ducci, G. Leo, and I. Favero, "Photoelastic coupling in gallium arsenide optomechanical disk resonators," Optics Express **22**, 14072 (2014).

[27] C. E. Rogers III, J. L. Carini, J. A. Pechkis, and P. L. Gould, "Characterization and compensation of the residual chirp in a Mach-Zehnder-type electro-optical intensity modulator," Optics Express **18**, 1166 (2010).

[28]T. J. Johnson, M. Borselli, and O. Painter, "Self-induced optical modulation of the transmission through a high-Q silicon microdisk resonator," Optics Express **14**, 817 (2006).
[29]D. A. Kleinman, R. C. Miller, and W. A. Nordland, "Two-photon absorption of Nd laser radiation in GaAs," Applied Physics Letters **23**, 243 (1973).
[30]S. Krishnamurthy, Z. G. Yu, L. P. Gonzalez, and S. Guha, "Temperature- and wavelength-dependent two-photon and free-carrier absorption in GaAs, InP, GaInAs, and InAsP," Journal of Applied Physics **109**, 033102 (2011).
[31]W. C. Hurlbut, K. L. Vodopyanov, P. S. Kuo, M. M. Fejer, and Y. S. Lee, "Multi-photon absorption and nonlinear refraction of GaAs in the mid-infrared," Optics Letter **32**, 668 (2007).
[32]T. Skauli, P. S. Kuo, K. L. Vodopyanov, T. J. Pinguet, O. Levi, L. A. Eyres, J. S. Harris, M. M. Fejer, B. Gerard, L. Becouarn, and E. Lallier, "Improved dispersion relations for GaAs and applications to nonlinear optics," Journal of Applied Physics **94**, 6447 (2003).
[33]F. G. Della Corte, G. Cocorullo, M. Iodice, and I. Rendina, "Temperature dependence of the thermo-optic coefficient of InP, GaAs, and SiC from room temperature to 600 K at the wavelength of 1.5 μm," Applied Physics Letters **77**, 1614 (2000).
[34]L. Ding, C. Baker, P. Senellart, A. Lemaitre, S. Ducci, G. Leo, and I. Favero, "High frequency GaAs nano-optomechanical disk resonator," Physical Review Letters **105**, 263903 (2010).
[35]J. S. Blakemore, "Semiconducting and other major properties of gallium arsenide," Journal of Applied Physics **53**, R123 (1982).

I. SUPPLEMENTARY MATERIAL

A. Supplementary Figures

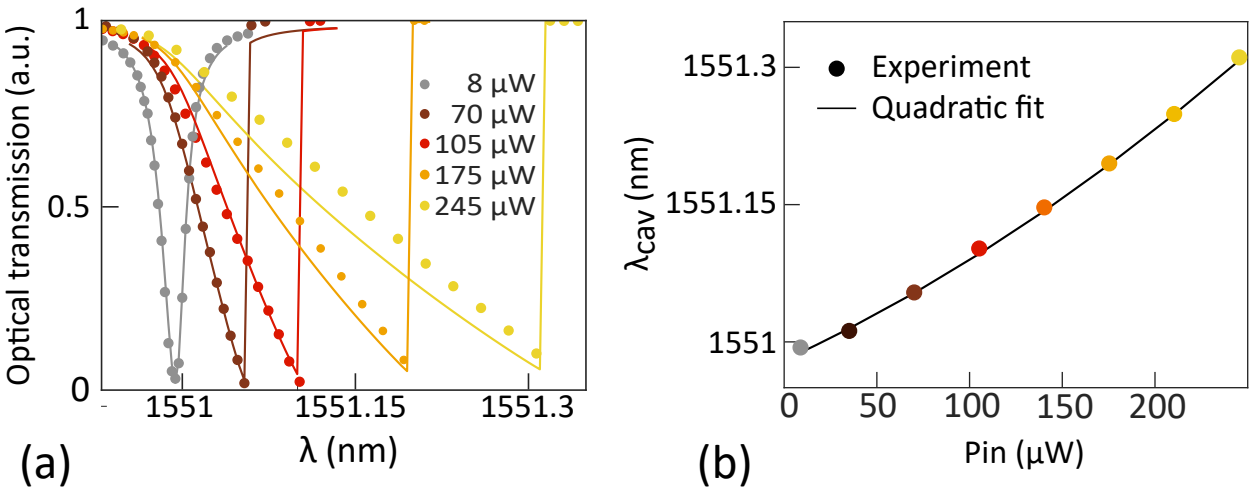

FIG. S1. (a) Measured (dots) and fitted (solid line) WGM optical response spectrum at different input powers, using the model introduced in Ref.[S1]. (b) The thermo-optic red-shift of the cavity resonant wavelength is quadratic in the input power P_{in}, revealing the effect of TPA.

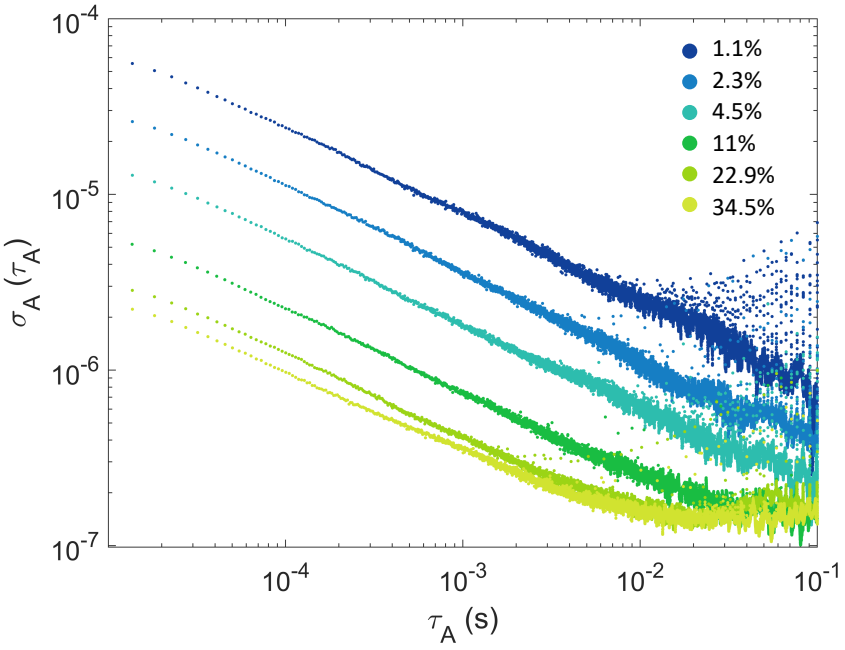

FIG. S2. Frequency stability of the driven optomechanical resonator at different modulation depths given as a percentage of the input power (2β in the main text). The Allan deviation is calculated following Ref.[S2]. A 10^{-7} frequency stability is obtained for the largest EOM driving voltage (750 mV, 34.5% of modulated input power), at 10 ms of integration time (τ_A).

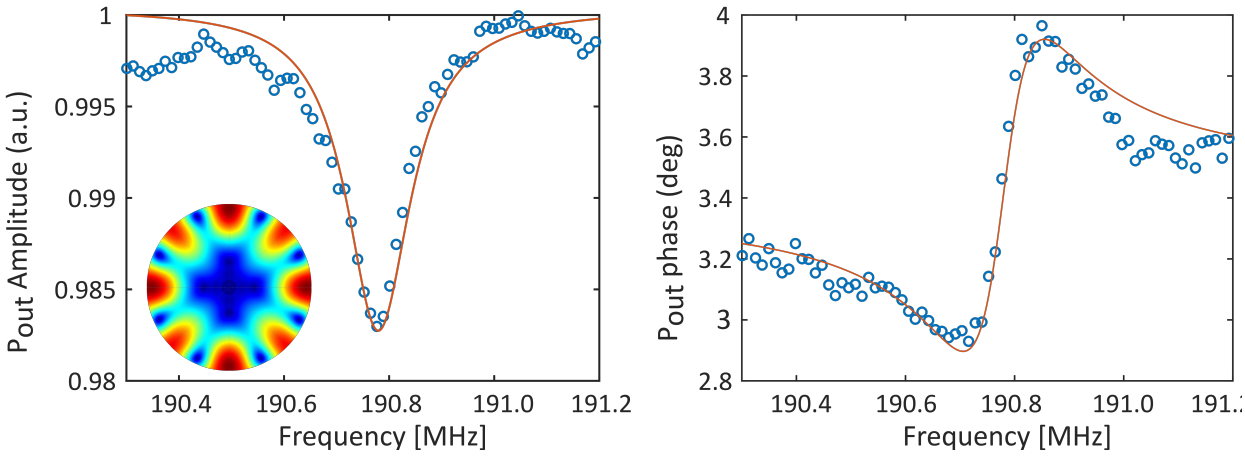

FIG. S3. Amplitude and phase of the demodulated output signal around 190 MHz. Dots represent experimental data, while the model is shown as a solid line. The total displacement profile of the mechanical mode is reported in inset. It belongs to the wine glass modes family.

B. Supplementary Equations

In presence of a small amplitude modulation of the input light at frequency Ω, the governing equations (Eq.3 of the main text) lead to the following relations:

$$\begin{aligned}
\left(i\Omega + i\bar{\Delta} - \frac{\kappa}{2}\right) A^- + i\left(g_{om}X + \frac{\omega_{cav}}{n_g}\frac{dn_{eff}}{dT}\Delta T_c\right)\bar{a} + \sqrt{\kappa_{ext}}\bar{a}_{in}\frac{\beta}{2} = 0,\\
\left(-i\Omega + i\bar{\Delta} - \frac{\kappa}{2}\right) A^+ + i\left(g_{om}X^* + \frac{\omega_{cav}}{n_g}\frac{dn_{eff}}{dT}\Delta T_c^*\right)\bar{a} + \sqrt{\kappa_{ext}}\bar{a}_{in}\frac{\beta}{2} = 0,\\
\frac{X}{\chi} - \hbar g_{om}\bar{a}\left(A^- + (A^+)^*\right) - \alpha\Delta T_c = 0,\\
\Delta T_c\left(i\Omega - \frac{1}{\tau_{th}}\right) + \frac{\hbar\omega_L R_{th}\kappa_{abs}}{\tau_{th}}\bar{a}(A^- + (A^+)^*) = 0,
\end{aligned} \tag{S1}$$

The resulting expressions of A^- and A^+ as function of the frequency Ω are given in the main text, while the temperature and displacement components are:

$$\Delta T_c(\Omega) = \frac{\hbar\omega_L R_{\rm th}(\kappa_{\rm lin} + 2\bar{\kappa}_{\rm TPA})\bar{a}}{1 - i\Omega\tau_{\rm th}} \times \frac{i\bar{\Delta}(\phi - \phi^*) + (\kappa/2 - i\Omega)(\phi + \phi^*)}{\bar{\Delta}^2 + \bar{\Delta}(\zeta_{\rm opt} + \zeta_{\rm th}) - (\Omega + i\kappa/2)^2} \tag{S2}$$

$$X(\Omega) = \chi(\Omega)\,\bar{a}\left(\hbar g_{\rm om} + \frac{\alpha\hbar\omega_L R_{th}(\kappa_{\rm lin} + 2\bar{\kappa}_{\rm TPA})}{1 - i\Omega\tau_{th}}\right)\frac{i\bar{\Delta}(\phi - \phi^*) + (\kappa/2 - i\Omega)(\phi + \phi^*)}{\bar{\Delta}^2 + \bar{\Delta}(\zeta_{\rm opt} + \zeta_{\rm th}) - (\Omega + i\kappa/2)^2} \tag{S3}$$

REFERENCES

[S1]D. Parrain, C. Baker, G. Wang, B. Guha, E. G. Santos, A. Lemaitre, P. Senellart, G. Leo, S. Ducci, and I. Favero, "Origin of optical losses in gallium arsenide disk whispering gallery resonators," Optics Express **23**, 19656 (2015).

[S2]D. W. Allan, "Time and frequency characterization estimation and prediction of precision clocks and oscillators," Ieee Transactions on Ultrasonics, Ferroelectrics and Frequency Control. **34**, 647 (1987).